Vibrational Dynamics of the I_3 Radical: A Semiempirical Potential Surface, and Semiclassical Calculation of the Anion Photoelectron Spectrum

C. J. Margulis, D. A. Horner, S. Bonella, and D. F. Coker*

Department of Chemistry, Boston University, 590 Commonwealth Avenue, Boston, Massachusetts 02215

Received: July 26, 1999; In Final Form: September 24, 1999

The semiempirical diatomics in molecules (DIM) approach is used to model the potential surface for ground-state vibration of a linear I_3 molecule. We use this system to explore semiclassical methods for treating quantal nuclear vibrations by computing the photoelectron spectrum of I_3^- which produces vibrationally excited I_3 . We compare semiclassical results with full quantum calculations and experimental results recently reported by Neumark and co-workers. (Taylor, T. R.; Asmis, K.R.; Zanni, M. T.; Neumark, D. M. *J. Chem. Phys.* **1999**, *110*, 7607.)

1. Introduction

Since the 1950s the existence of the triiodide radical has been proposed as an intermediate species to explain how iodine atoms, produced by photodissociating I_2, can recombine in the gas phase to reproduce the diatomic species. The accepted mechanism involves an $I^\bullet$ radical first colliding I_2 to form stable I_3 which subsequently undergoes collision with another $I^\bullet$ radical, then this collision complex breaks apart to give two I_2 molecules. Despite its proposed importance in this most fundamental reaction of gas-phase chemical kinetics, direct experimental observation of the I_3 molecule has only very recently been accomplished in the high-resolution photoelectron spectroscopy studies of Neumark and co-workers.[1]

The first goal of this paper is to demonstrate that a very simple description of the I_3 molecule offered by the semiempirical diatomics-in-molecules (DIM) approach is actually capable of providing a very reliable representation of this molecule, reproducing the recently measured binding energies, and vibrational frequencies with surprising accuracy.

Next we summarize how time dependent perturbation theory can be used to compute the distribution of ejected photoelectron kinetic energy $P_\beta(\epsilon)$ in the thermal equilibrium photoelectron spectrum of I_3^- in which vibrationally hot I_3 is produced according to the following process:

$$I_3^-(\text{therm}) + \hbar\nu \rightarrow I_3(\text{vib}) + e^-(\epsilon) \qquad (1)$$

Finally we will compare the results of fully quantum dynamical calculations of this photoelectron spectrum, with classical and semiclassical calculations of the I_3 vibrational dynamics probed by these measurements, and we compare our theoretical results with the experimental photoelectron spectrum of Neumark and co-workers.[1]

2. Methods

2.1. A DIM Potential Model for Ground Electronic State Intramolecular Vibrations of I_3. The model assumes that the I_3 molecule is linear, hence the projection of the total angular momentum of the system into the molecular axis is a good quantum number. Following the same scheme used in previous work[2] we write the basis set as Hund's case C kets

$$|J_1 m_{j1}\rangle|J_2 m_{j2}\rangle|J_3 m_{j3}\rangle = |J_1 m_{j1}, J_2 m_{j2}, J_3 m_{j3}\rangle$$

where J_k and m_{jk} are the total angular momentum and it's projection on the molecular axis for each of the iodine atoms. Our purpose in this paper is to focus on the properties of the ground electronic state of I_3, hence we will reduce our basis set to a minimum subspace that will include only the necessary kets mixing to form this lowest energy eigenstate. Thus the approach we present here will not produce all the subsequent excited states, but only some of them.

We suppose that the ground-state eigenket has total angular momentum projection

$$M_J = \sum_{k=1}^{3} m_{jk} = \pm{}^1/_2$$

so only kets satisfying this condition will combine to generate this assumed lowest energy eigenstate.[3] Our knowledge of the ground-state dissociation limits of the I_3 radical can be used to further limit the basis set. Thus if one of the bonds is stretched, the molecule should dissociate to ground-state I_2 and an $I^\bullet$ radical species. The ground state of I_2 in our representation is

$$1/\sqrt{2}(|{}^3/_2, {}^1/_2\rangle|{}^3/_2, -{}^1/_2\rangle - |{}^3/_2, -{}^1/_2\rangle|{}^3/_2, {}^1/_2\rangle)$$

and the $I^\bullet$ radical ground state is

$$|{}^3/_2 \pm {}^1/_2\rangle$$

These considerations thus enable us to limit the basis kets to only those having all the $J_k = {}^3/_2$ and the $m_{jk} = \pm{}^1/_2$. This procedure is only valid in the gas phase, in solution other states that we are not including in the calculations described here will be coupled by anisotropic interactions with the solvent and thus make contributions to the lowest energy solution phase eigenket, but this is beyond the scope of the current paper.

The DIM Hamiltonian operator has the form[4,5]

$$\sum_{i<j} \hat{H}_{i,j} - n\sum_i \hat{H}_i \qquad (2)$$

and we choose the zero in energy to be that of the isolated $I^\bullet$ radicals; therefore, the second sum in the above expression can be disregarded. For convenience in the notation we will drop the J index in the angular momentum expression since it is the

10.1021/jp992596m CCC: $18.00
Published on Web 11/06/1999

same for all iodine atoms and we will only label them by their values of m_{jk}.

In the gas phase the I_3 ground state can have total $M_J = \pm 1/2$, both angular momentum orientation states are degenerate and uncoupled, thus we need only consider the one with total $M_J = 1/2$. The only basis kets to consider now are the following:

$$\{|-1/2,1/2,1/2\rangle;\quad |1/2,-1/2,1/2\rangle;\quad |1/2,1/2,-1/2\rangle\}$$

Any matrix element between them will be of the form

$$\langle m_{j1},m_{j2},m_{j3}|\hat{H}_{l,m}|m'_{j1},m'_{j2},m'_{j3}\rangle = \langle m_{jl},m_{jm}|\hat{H}_{l,m}|m'_{jl},m'_{jm}\rangle \times \langle m_{jn}|m'_{jn}\rangle$$

i.e., an I_2 matrix element times a $\delta(m_j,m'_j)$.

The full electronic Hamiltonian matrix thus becomes

$$\langle -1/2,1/2,1/2|\hat{H}|-1/2,1/2,1/2\rangle = \langle -1/2,1/2|\hat{H}_{R1}|-1/2,1/2\rangle + \langle 1/2,1/2|\hat{H}_{R2}|1/2,1/2\rangle + \langle -1/2,1/2|\hat{H}_{R3}|-1/2,1/2\rangle$$

$$\langle 1/2,-1/2,1/2|\hat{H}|1/2,-1/2,1/2\rangle = \langle 1/2,-1/2|\hat{H}_{R1}|1/2,-1/2\rangle + \langle -1/2,1/2|\hat{H}_{R2}|-1/2,1/2\rangle + \langle 1/2,1/2|\hat{H}_{R3}|1/2,1/2\rangle$$

$$\langle 1/2,1/2,-1/2|\hat{H}|1/2,1/2,-1/2\rangle = \langle 1/2,1/2|\hat{H}_{R1}|1/2,1/2\rangle + \langle 1/2,-1/2|\hat{H}_{R2}|1/2,-1/2\rangle + \langle 1/2,-1/2|\hat{H}_{R3}|1/2,-1/2\rangle$$

$$\langle -1/2,1/2,1/2|\hat{H}|1/2,-1/2,1/2\rangle = \langle -1/2,1/2|\hat{H}_{R1}|1/2,-1/2\rangle$$

$$\langle -1/2,1/2,1/2|\hat{H}|1/2,1/2,-1/2\rangle = \langle -1/2,1/2|\hat{H}_{R3}|1/2,-1/2\rangle$$

$$\langle 1/2,-1/2,1/2|\hat{H}|1/2,1/2,-1/2\rangle = \langle -1/2,1/2|\hat{H}_{R2}|1/2,-1/2\rangle$$

Where R1 is the distance from the I atom at one end of the molecule to the central one, R2 is the distance from the I atom at the other end to the central atom, and R3 is the distance between the two I atoms at opposite ends of the molecule. Using Table 1 in ref 2 and performing some simple algebra we find the matrix elements to be

$$\langle -1/2,1/2|\hat{H}|-1/2,1/2\rangle = 1/2(E(1^3\Sigma_u^+) + E(X))$$

$$\langle 1/2,1/2|\hat{H}|1/2,1/2\rangle = E(^1\Pi_u)$$

for which experimental values are available in Batista and Coker's[2] paper and the references therein.

The electronic ground-state surface of I_3 is thus obtained by simply diagonalizing the 3×3 matrix whose elements are summarized above and selecting the lowest energy eigenvalue. In Figure 1 we display the elements of our reduced DIM Hamiltonian matrix as functions of R1 and R2 while Figure 2 shows the electronic ground state of I_3 calculated from these matrix elements as described above. Table 1 summarizes various properties of this ground-state I_3 potential and compares these results with the experimental values.[1] This table also summarizes various properties of the I_3^- potential which we need to prepare the initial state for our photoelectron spectrum studies.

The symmetric stretch frequency of I_3 obtained from these calculations is about 10% too high, and the dissociation energy to I_2 and an $I^\bullet$ radical is also a little high but with in the reported experimental uncertainty. Given the shapes of the various diabats and coupling matrix elements presented in Figure 1, the accuracy with which our DIM ground-state surface reproduces experimental values is quite remarkable.

TABLE 1: Comparison of Properties of Calculated DIM Surface for I_3 with Experimental Results[a]

item	parameters and results: this paper	parameters and results: Neumark's results
symmetric frequency	126.1 cm^{-1}	115 ± 5 cm^{-1}
antisymmetric frequency	163.7 cm^{-1}	
dissociation energy $I_3 \rightarrow I_2 + I^\bullet$	0.19157 eV	0.143 ± 0.06 eV
dissociation energy $I_3 \rightarrow 3\ I^\bullet$	1.74723 eV	
I_3 equilibrium bond length	2.762 Å	
I_3 adiabatic EA	4.226 eV	4.226 eV
I_3^- symmetric frequency[b]	106.7 cm^{-1}	112 cm^{-1}
I_3^- antisymmetric frequency	122.2 cm^{-1}	
-I_3^- bond length	2.85 Å	
τ	100 fs	
$\hbar\omega$	4.657 eV	4.657 eV

[a] The I_3^- potential is assumed to be quadratic in both symmetric and antisymmetric coordinates to simplify the calculations. [b] Different values for the symmetric and antisymmetric frequencies can be found in the literature. See refs 6 and 7 and references therein.

Our calculations assume that the I_3 molecule is linear and symmetric just like I_3^-. Thus the fact that the equilibrium bond length we find for our model I_3 molecule is about 0.1 Å shorter than that of the parent I_3^- means that when we photoionize the anion via a vertical Franck−Condon excitation we will extend the symmetric stretch mode of the resulting I_3. As we shall see in the detailed analysis of our calculated signals we present in section 3, antisymmetric stretch components can enter our signals through thermal populations of ground electronic state antisymmetric stretch motions or through nonlinear couplings between the symmetric and antisymmetric modes as a result of motion over our fully nonlinearly coupled I_3 potential surface.

2.2. Semiclassical Computation of the Photoelectron Spectrum. For our purposes we view the photoionization reaction

$$A^-(I) + \hbar\omega \rightarrow A(F) + e^-(\epsilon) \qquad (3)$$

as a process which takes the molecular ion system A^- from a discrete electronic state Φ_I to a continuum molecular ion electronic state $\Phi_{F\epsilon}$ by absorption of a photon. The final continuum state is really a neutral molecule A in one of its discrete states Φ_F and an ejected free electron with continuous kinetic energy ϵ. In the appendix we outline the time dependent perturbation theory approach to computing the probability of observing ejected photoelectrons with kinetic energy ϵ obtained by ionizing molecules prepared in a thermal distribution of vibrational states moving on the ground electronic surface of I_3^- (state I) and producing ground-state neutrals (state F). There we show that if we assume that the dipole matrix elements connecting states I and F depend weakly on nuclear coordinates and vary slowly with electronic kinetic energy, ϵ, (see appendix for details), this probability is obtained as

$$P_\beta^{IF}(\epsilon) \sim \mathrm{Re}\left\{\int_0^\infty dt \phi_{IF}(t;\beta) \exp\left[-\frac{i}{\hbar}(\epsilon - \hbar\omega)t\right] \exp\left[-\frac{t^2}{4\tau^2}\right]\right\} \qquad (4)$$

where the thermally averaged dynamical correlation function appearing in this expression is given by

$$\phi_{IF}(t;\beta) = \sum_{\mathbf{v}} \exp[-\beta E_{I\mathbf{v}}] \exp\left[\frac{i}{\hbar}E_{I\mathbf{v}}t\right] f_{F,I\mathbf{v}}(t) \qquad (5)$$

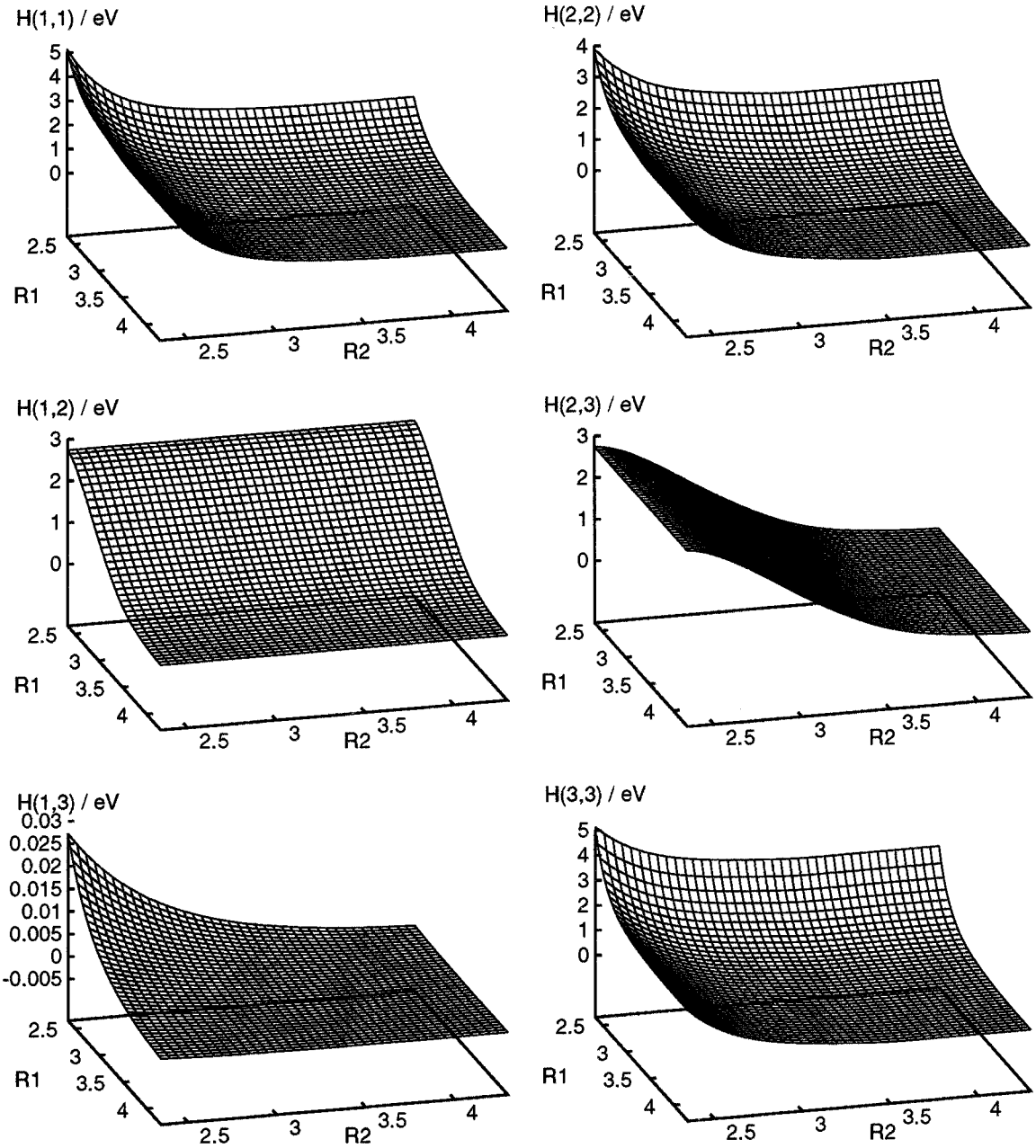

Figure 1. Elements of the DIM Hamiltonian used in our calculation of the collinear ground state electronic surface of I_3 as a function of bond lengths in Ångstroms.

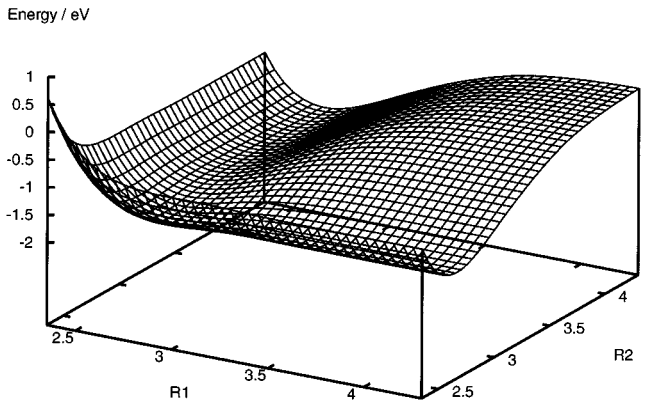

Figure 2. DIM Ground-state electronic surface of I_3 as a function of bond lengths in Ångstroms.

Here E_{Iv} is the energy of the **v**th vibrational eigenstate on the initial electronic surface I, $\chi_{Iv}(\mathbf{Q})$ is the corresponding nuclear vibrational eigenstate on this surface, and the individual vibrational component, excited electronic state propagated correlation functions are

$$f_{F,Iv}(t) = \left\langle \chi_{Iv} \middle| \exp\left[-\frac{i}{\hbar}\hat{H}_F t\right] \middle| \chi_{Iv} \right\rangle \tag{6}$$

where $\hat{H}_F$ is the Hamiltonian governing nuclear dynamics over the excited electronic state potential F. This correlation function thus involves propagating the nuclear vibrational eigenstates of the initial electronic surface over the final excited-state surface and measuring the overlap of these propagated function at time t with the initial wave function.

In our studies we will assume that the initial electronic surface of the I_3^- can be approximated harmonically around its equilibrium geometry and that this approximation will be reliable for all the thermally accessible initial vibrational states at the temperatures of interest. This approximation is expected to be

reasonable for the deep I_3^- ground-state surface. However, vibrations on the I_3 excited state surface are expected to be highly anharmonic as motion on this surface is only very weakly bound along certain directions as seen in Figure 2.

To simplify our calculations, we further assume that the bending of the I_3 molecule is not excited in these experiments and that rotation−vibration coupling can be ignored. Thus we need only the symmetric and antisymmetric stretch coordinates to describe the anharmonic intramolecular vibrational dynamics on the I_3 potential surface. This reduces our intramolecular vibrational problem to just two dimensions. We thus employ the initial ground state normal mode coordinates of the system in our quantum and semiclassical propagation calculations detailed below.

The individual vibrational correlation functions given in eq 6 can be computed exactly using standard FFT grid propagation methods[8,9] and the results added according to eq 5 to give the required thermal average correlation function. Such methods are, however, generally only viable for systems of few dimensions. Semiclassical methods based on propagating swarms of classical trajectories and carefully adding up the semiclassical phases associated with these trajectories to compute the approximate semiclassical dynamical wave function are in principle applicable to systems with many more dimensions.

We now consider the implementation of the Herman−Kluk, coherent state semiclassical propagator[10−16] to compute the correlation functions given above. With this approach the propagator describing nuclear vibrations on surface F has the form

$$\exp\left[-\frac{i}{\hbar}\hat{H}_F t\right] = \int \frac{d\mathbf{P}}{(2\pi\hbar)^d} d\mathbf{Q} |\mathbf{P}_t\mathbf{Q}_t\rangle C(\mathbf{P},\mathbf{Q},t) \exp\left[\frac{i}{\hbar}S(\mathbf{P},\mathbf{Q},t)\right]\langle\mathbf{P}\mathbf{Q}| \quad (7)$$

where the coordinate state representation of the time dependent coherent state basis set elements used in this description are the Gaussian functions

$$\langle\mathbf{x}|\mathbf{P}_t\mathbf{Q}_t\rangle = \left(\frac{2\gamma}{\pi}\right)^{d/4} \exp\left[-\gamma(\mathbf{x}-\mathbf{Q}_t)^2 + \frac{i}{\hbar}\mathbf{P}_t\cdot(\mathbf{x}-\mathbf{Q}_t)\right] \quad (8)$$

whose time dependent center position $\mathbf{Q}_t$, and phase $\mathbf{P}_t$ parameters are the positions and momenta of simple classical trajectories, γ is a constant arbitrary width parameter, $S(\mathbf{P},\mathbf{Q},t) = \int dt \mathbf{P}_t^2(\mathbf{P},\mathbf{Q})/2M - E_F(\mathbf{Q}_t(\mathbf{P},\mathbf{Q}))$ is the classical action along the trajectory propagated over our final state surface, which depends on the initial position $\mathbf{Q}$, and phase (momentum) $\mathbf{P}$ of the given basis function, and the function $C(\mathbf{P},\mathbf{Q},t)$ is related to the stability of the classical trajectory with respect to variations in initial conditions as measured by the so-called monodromy matrixes whose elements have the form $\mathbf{M}_{PQ}^{(ij)}(\mathbf{P},\mathbf{Q},t) = [\partial P_t^i/\partial Q^j](\mathbf{P},\mathbf{Q},t)$, for example. In all the calculations reported in this paper we have used ensembles containing 1000 trajectories. The quantity $C(\mathbf{P},\mathbf{Q},t)$ which weights each trajectory's contribution to the semiclassical propagator in eq 7 is found to have the form

$$C(\mathbf{P},\mathbf{Q},t) = \left\{\det\left[\frac{1}{2}\left(\mathbf{M}_{PP} + \mathbf{M}_{QQ} - 2\gamma i\hbar\mathbf{M}_{QP} + \frac{i}{2\gamma\hbar}\mathbf{M}_{PQ}\right)\right]\right\}^{1/2} \quad (9)$$

The monodromy matrixes can be computed by integrating the following auxiliary equations of motion which are determined by the time dependent local curvature of the potential along the classical trajectory

$$\dot{\mathbf{M}}_{QQ} = \mathbf{N}\mathbf{M}_{PQ} \qquad \dot{\mathbf{M}}_{PQ} = -\mathbf{D}(t)M_{QQ} \quad (10)$$

$$\dot{\mathbf{M}}_{QP} = \mathbf{N}\mathbf{M}_{PP} \qquad \dot{\mathbf{M}}_{PP} = -\mathbf{D}(t)M_{QP} \quad (11)$$

Where $\mathbf{N}$ is a diagonal matrix with elements equal to the inverses of the masses associated with the different particle coordinates, and $\mathbf{D}(t)$ is the time dependent Hessian matrix $D^{(ij)}(t) = [\partial^2 V/\partial Q^i \partial Q^j](\mathbf{Q}_t)$ computed at points along the classical trajectory.

Using the excited-state semiclassical nuclear propagator in eq 7 we can express the correlation functions in eq 6 as

$$f_{F,I\mathbf{v}}^{SC}(t) = \int \frac{d\mathbf{P}}{(2\pi\hbar)^d} d\mathbf{Q} \langle\chi_{I\mathbf{v}}|\mathbf{P}_t\mathbf{Q}_t\rangle C(\mathbf{P},\mathbf{Q},t) \times \exp\left[\frac{i}{\hbar}S(\mathbf{P},\mathbf{Q},t)\right]\langle\mathbf{P}\mathbf{Q}|\chi_{I\mathbf{v}}\rangle \quad (12)$$

Here the classical trajectories swarm over the potential surface associated with the final electronic state F.

With the assumptions described earlier, our vibrational eigenstates on surface I are products of harmonic oscillator eigenfunctions in the symmetric and antisymmetric coordinates. We can readily calculate the projections of these states onto our coherent state basis set in these coordinates and after some algebra we find for a given mode

$$\langle PQ|\chi_{Iv}\rangle = \frac{N_v}{\alpha}\left(\frac{2\gamma}{\pi}\right)^{1/4} \exp[-\gamma\alpha^2\delta(Q-X_0)^2] \times \exp[-\delta P^2/2\hbar^2] \exp[i\alpha^2\delta P(Q-X_0)] \sum_{n=0}^{v} (\alpha^2\delta)^{(n+1)/2} c_n P_n(g) \quad (13)$$

where the harmonic oscillator wave functions have the form $\psi_v(x) = N_v H_v(\alpha(x - x_0)) \exp[-\alpha^2(x - x_0)^2/2]$ with $\alpha = \sqrt{m\omega/\hbar}$, $N_v = (\alpha\sqrt{\pi}2^v v!)^{-1/2}$ is a normalization constant, $H_v(y) = \sum_0^v c_n y^n$ are the hermite polynomials, and $\delta = (2\gamma + \alpha^2)^{-1}$. The polynomials $P_n(g)$ result from the integrations and generally satisfy the recursion relation $P_{n+1}(g) = gP_n(g) + (n - 1)P_{n-1}(g)$ with $P_0 = 1$ and $P_1 = g$ and $g = \sqrt{\delta}[2\gamma(Q - x_0) - iP/\hbar]$.

Despite the appeal of obtaining semiclassical quantum dynamical effects by just averaging various dynamical quantities over an ensemble of classically propagating trajectories labeled by their initial conditions as, for example, in eq 12, the implementation of such semiclassical expressions is plagued with many serious numerical "traps for new players". In the discussion that follows we show how these problems arise in our application to the dynamics of I_3 excited in the photoelectron ejection experiments on I_3^-.

The main difficulty with implementing these semiclassical methods arises due to the rapid oscillation of the integrand in eq 12, for example, between positive and negative values in various regions of initial phase space point $(\mathbf{P},\mathbf{Q})$. In these rapidly oscillatory regions contributions from near-by trajectories should add destructively to give only a vanishingly small contribution to the final integral. The integration over points $(\mathbf{P},\mathbf{Q})$ which we accomplish by summing over the ensemble of trajectories thus requires a sufficiently dense packing of trajectories in such regions to accurately represent this cancellation. The primitive implementation of a grid or Monte Carlo based approach thus wastes much effort propagating trajectories from such regions only to have them add destructively to represent zero.

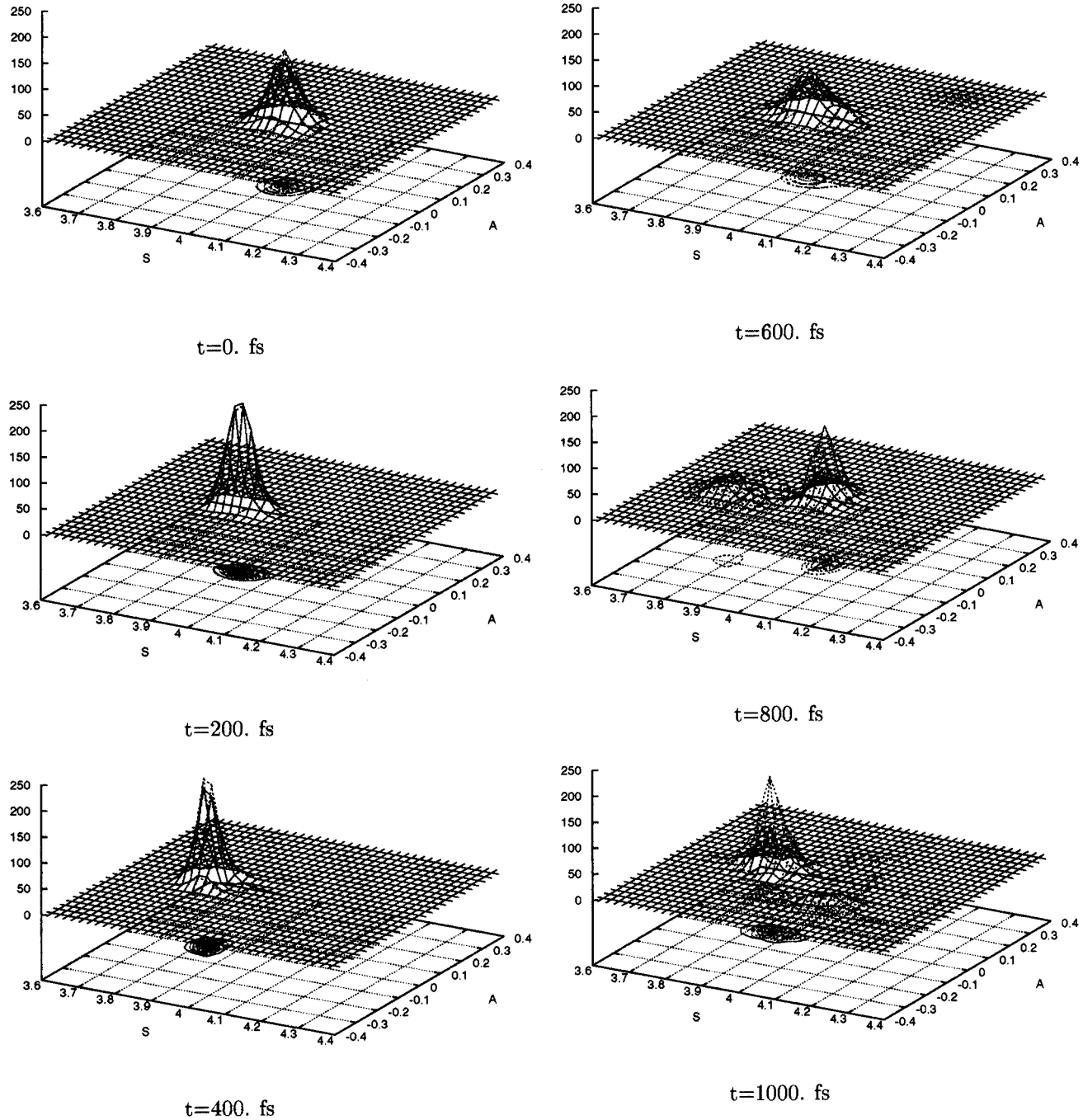

Figure 3. Propagation of initial harmonic I_3^- ground vibrational state on the photoexcited I_3 DIM potential surface. Surface of solid lines is propagated using the bare Herman-Kluk semiclassical algorithm. The dashed surface is the full quantum wave function propagated using split operator FFT methods. The wave functions are plotted as functions of symmetric and antisymmetric stretch normal modes in Ångstroms.

The situation with a semiclassical integrand like that in eq 12 is even more troublesome. The phase factor in the integrand $\exp[i\theta(\mathbf{P},\mathbf{Q})/\hbar]$, say, becomes a rapidly oscillatory function of $(\mathbf{P},\mathbf{Q})$ because the phase, $\theta(\mathbf{P},\mathbf{Q})$, varies with $(\mathbf{P},\mathbf{Q})$ and dividing by a small $\hbar$ amplifies these variations into rapid oscillations of the phase factor. In stationary phase regions where the rate of change of $\theta(\mathbf{P},\mathbf{Q})$ with $(\mathbf{P},\mathbf{Q})$ remains sufficiently small there will be constructive interference between trajectories giving nonvanishing contributions. Outside these stationary phase regions, however, the phase starts to change and the lowest order variation in phase is easily shown to be determined by the monodromy matrixes $M_{\mathbf{Q},\mathbf{P}} = \partial\mathbf{Q}_t/\partial\mathbf{P}$, for example. In the classical dynamics of anharmonic many-body systems such quantities can become very large very quickly as trajectories become exponentially unstable with respect to variations in their initial conditions in classically chaotic regions[4,17−26] Semiclassical expressions like that in eq 12 usually involve weighting trajectory contributions by quantities such as $C(\mathbf{P},\mathbf{Q})$ which depend on potentially diverging monodromy factors. As discussed above these explosive monodromy factors also appear exponentially in the phase factor so the cancellation of their contribution is crucial.

Several approaches for handling the cancellation of nonstationary trajectories and removing their explosive consequences in systems exhibiting strongly chaotic classical dynamics have recently been presented.[14,18−25] All these methods are based on the ideas of stationary phase filtering which were developed during the 1980's when attempts were made to use path integral Monte Carlo methods to compute fully quantum real time correlation functions.[27−31]

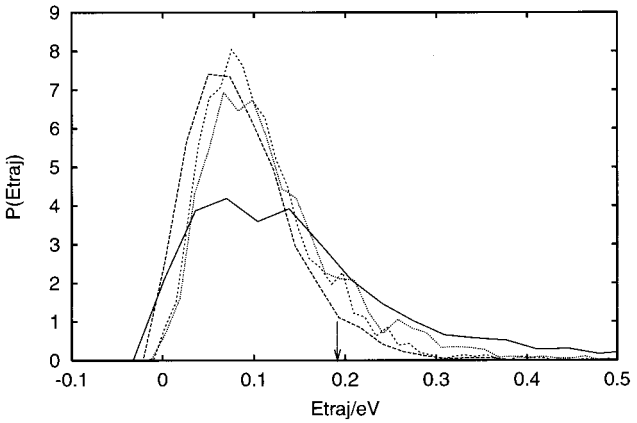

Figure 4. Classical trajectory energy distributions for various values of coherent state parameter γ for propagation on I_3 surface. The I_3 potential minimum is zero energy and the negative energies are due to the low energy resolution of our histogram. The dissociation energy of our model is indicated by the arrow. Values of γ in $Å^{-2}$ displayed are $\gamma = 25$. (solid), $\gamma = 125$. (long dashes), $\gamma = 525$. (short dashes), $\gamma = 825$. (dots). In our calculations we employ a value of $\gamma = 125$, which gives a trajectory energy distribution with a smaller high energy tail to reduce the rapid growth of chaotic trajectories in our ensemble.

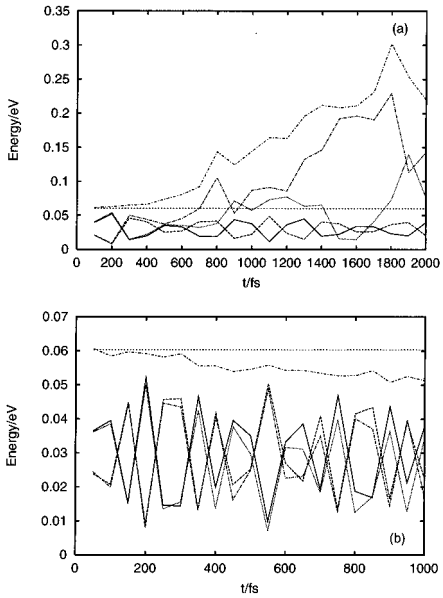

Figure 5. (a) Comparison of time dependence of total quantum system energy and kinetic and potential components computed using full quantum propagation (curves add to give total energy conservation), and results computed using the bare Herman-Kluk semiclassical approach which show serious energy conservation problems and divergence from exact quantum results beyond 300−400 fs. (b) Similar comparison to a only here results from preaveraging semiclassical calculations show much better energy conservation and comparison with full quantum results.

The particular method we have found convenient to implement is that due to Herman[22,23] and we now present a brief summary of the approach and demonstrate how it remedies the serious problems arising from classical chaos even in a system as simple as the two coupled anharmonic stretching modes of I_3.

The disasterous effects of classical chaos on the straightforward implementation of semiclassical expressions such as that in eq 12 for I_3 can be seen very clearly in Figure 3 where we compare the full quantum and semiclassical time dependent normalized wave function densities for symmetric and antisymmetric stretch coordinates of I_3 produced after photoelectron ejection from I_3^-. The initial Gaussian density produced during the Franck−Condon excitation of our harmonic model of I_3^- starts out on the attractive wall of the I_3 surface with the symmetric stretch coordinate extended relative to the equilibrium geometry of I_3 due to the differences in equilibrium bondlength for the ionic and neutral species which are accurately produced by our model surfaces.

This nonequilibrium excited state distribution thus first compresses in the symmetric stretch and then as it extends in this direction the density also shows elongation in the antisymmetric stretch direction due to the strong anharmonic couplings between these modes present in our DIM model I_3 surface.

In Figure 4 we present the distribution of classical trajectory energies for various coherent state basis set width parameters γ. We see that as this basis set width parameter is varied, the energy distribution of our classical trajectory ensemble changes considerably. The value of this parameter we used in most of our calculations was $\gamma = 125$ $Å^{-2}$. This value gives a narrow energy distribution with a small tail extending above the smallest dissociation energy of our potential ($D_{anti} \sim 0.2$ eV).

The longer time wave functions ($t > 400$ fs) presented in Figure 3 show a serious discrepancy between the wave function obtained from the bare application of the semiclassical coherent state basis set approach and the exact wave function. These semiclassical results at the longer times show wave function fragmentation resulting from a few trajectories in the high energy tail of the distribution in Figure 4 exhibiting large amplitude motions. These high energy trajectories rapidly become unstable with respect to variations in their initial conditions so the magnitudes of their $C(\mathbf{P},\mathbf{Q},t)$ weights in the bare semiclassical expression (eq 12) become overwhelming. In Figure 5a we show the time history of the kinetic, potential, and total energy computed using the bare semiclassical wave function and the fully quantum result. As expected, beyond 400 fs, the semiclassical energy components deviate dramatically from the exact results and the total energy of the bare semiclassical propagated wave function shows serious conservation problems. Not surprisingly, since the ensemble average is becoming dominated by the unstable high energy components due to their rapidly growing $C(\mathbf{P},\mathbf{Q},t)$ factors, the energy trends upward to the average of these high energy trajectories (see Figure 4).

If we were free to increase the ensemble size without bound the contribution from these unstable trajectories would eventually be approximately canceled by interference with other unstable trajectories since they eminate from nonstationary regions of phase space as discussed earlier. Such an approach is in general numerically impractical as it requires the cancellation of very large weights with different signs.

The approach adopted in the so-called "integrand conditioning" or "preaveraging" methods attempts to average these large interferring weights over many close lying trajectories by assuming a linear or quadratic variation of the phase around a trajectory, and within this approximation intergrating the weight analytically to obtain a "pre-averaged" weight which no longer oscillates wildly.[18,19−21,23,32,33]. Typically these methods first multiply the integral being evaluated by unity represented as a normalized integral of a Gaussian in the difference between the original integration variables and the preaveraging Gaussian integral variables. If the widths of these preaveraging Gaussians are made small enough, the phase of the original integrand can be expanded to low order in the difference variables and the resulting Gaussian integrals performed analytically to give an averaged weight (see for example refs 22 and 23 for details).

The main advantage of the specific preaveraging approach developed by Herman[22,23] is that it preserves the shape of the fixed width coherent state basis set used to represent the time evolving wave function. This is accomplished by changing the integration variables in the semiclassical expression like eq 12 from the trajectory initial phase space point ($\mathbf{P},\mathbf{Q}$) to the final point variables ($\mathbf{P}_t,\mathbf{Q}_t$), the Jacobian of this transformation is unity. The integrand conditioning Gaussian integrals are then introduced in displacements of the final points of the trajectories. Thus we multiply our semiclassical expression by the following representation of unity

$$\prod_{k=1}^{d}\left(\frac{c_P^k c_Q^k}{\pi^2}\right)^{1/2}\int \mathrm{d}p_t^k \int \mathrm{d}q_t^k \exp[-c_P^k(P_t^k - p_t^k)^2] \times \exp[-c_Q^k(Q_t^k - q_t^k)^2] = 1 \quad (14)$$

By choosing these preaveraging Gaussians to be sufficiently narrow (making the c_P^k and c_Q^k appropriately large for the various degrees of freedom, k) we can truncate the expansion of the phase of the semiclassical integrand in final point displacements to low order and perform the preaveraging integrals analytically. The final result is obtained by returning to an expression involving integrals over trajectory initial conditions but the weights of the different trajectories must be determined by reverse propagating the auxiliary trajectory stability equations from the final points reached by each trajectory. For the results reported here we have employed Herman's first order preaveraging form in which an initial function whose coherent state representation has the form $\langle \mathbf{PQ}|\psi_0\rangle = |\langle \mathbf{PQ}|\psi_0\rangle| \exp[i\theta_0/\hbar]$ is propagated according to the result

$$|\psi_t\rangle = \int \frac{\mathrm{d}\mathbf{P}}{(2\pi\hbar)^d}\mathrm{d}\mathbf{Q}|\mathbf{P}_t,\mathbf{Q}_t\rangle C(\mathbf{P},\mathbf{Q},t)\exp\left[\frac{i}{\hbar}S(\mathbf{P},\mathbf{Q},t)\right] \times \exp[-\Delta\theta^2(\mathbf{P},\mathbf{Q},t)]\langle \mathbf{PQ}|\psi_0\rangle \quad (15)$$

Here the exponent in the preaveraging weight factor has the form

$$\Delta\theta^2(\mathbf{P},\mathbf{Q},t) = \sum_{k=1}^{d}\left\{\left(\frac{1}{4\hbar^2 c_P^k}\right)\left(\frac{\partial\theta}{\partial P_t^k}\right)^2(\mathbf{P},\mathbf{Q},t) + \left(\frac{1}{4\hbar^2 c_P^k}\right)\left(\frac{\partial\theta}{\partial Q_t^k}\right)^2(\mathbf{P},\mathbf{Q},t)\right\} \quad (16)$$

For the coherent state basis set we find that the phase derivatives in the above expression are the components of the following vectors

$$\frac{\partial\theta}{\partial\mathbf{Q}_t} = \left(\frac{\partial\theta_0}{\partial\mathbf{Q}} - \mathbf{P}\right)^T\frac{\partial\mathbf{Q}}{\partial\mathbf{Q}_t} + \left(\frac{\partial\theta_0}{\partial\mathbf{P}}\right)^T\frac{\partial\mathbf{P}}{\partial\mathbf{Q}_t} \quad (17)$$

and

$$\frac{\partial\theta}{\partial\mathbf{P}_t} = \left(\frac{\partial\theta_0}{\partial\mathbf{Q}} - \mathbf{P}\right)^T\frac{\partial\mathbf{Q}}{\partial\mathbf{P}_t} + \left(\frac{\partial\theta_0}{\partial\mathbf{P}}\right)^T\frac{\partial\mathbf{P}}{\partial\mathbf{P}_t} \quad (18)$$

In these expressions we assume that all terms which do not contain the time reversed monodromy matrixes ($\partial\mathbf{Q}/\partial\mathbf{P}_t$, for example) are small and can be ignored compared to these factors which grow exponentially in systems exhibiting chaotic dynamics.

The more conventional approach,[20] on the other hand, introduces the preaveraging Gaussians in initial point displacements resulting in a travelling coherent state basis set in which the coherent state widths vary in different ways along different trajectories. If the coherent state basis elements get very narrow many trajectories may be needed to represent the dynamical wave function in these regions. Generally with this approach, however, the preaveraged weights of the trajectories associated with these narrow coherent state basis elements are small so they make little contribution anyway. This deterioration of the basis set is avoided with Herman's frozen Gaussian approach.

The approach we use to implement preaveraging can thus be summarized as follows: (1) Trajectory initial conditions ($\mathbf{P},\mathbf{Q}$) are first sampled from the distribution $|\langle \mathbf{PQ}|\psi_0\rangle|$. Each initial condition generated in this way is given an initial weight $\exp[i\theta_0(\mathbf{P},\mathbf{Q})/\hbar]$. (2) Next these trajectories are evolved classically to phase space points ($\mathbf{P}_t,\mathbf{Q}_t$) at time t. At this point we evaluate the coherent state representation of whatever function concerns us for our time correlation function. Along each trajectory we compute the classical action S and weight each trajectory's contribution by $\exp[iS/\hbar]$. (3) Now we must compute the preaveraging weight based on the time reversed monodromy factors appearing in eq 17. This is accomplished by setting the monodromy matrixes to the appropriate unit or zero matrixes at time t and reverse time integrating eq 10 back $t = 0$. This reverse time integration requires the evaluation of the Hessian at all points along each classical trajectory. It can be shown[23,34] that the $C(\mathbf{P},\mathbf{Q},t)$ weighting factors can be computed from these reverse propagated monodromy matrixes according to the following result

$$C(\mathbf{P},\mathbf{Q},t) = \left\{\det\left[\frac{1}{2}\left(\tilde{\mathbf{M}}_{PP} + \tilde{\mathbf{M}}_{QQ} + 2\gamma i\hbar\tilde{\mathbf{M}}_{QP} - \frac{i}{2\gamma\hbar}\tilde{\mathbf{M}}_{PQ}\right)\right]\right\}^{1/2} \quad (19)$$

with $\tilde{\mathbf{M}}_{QP}^{(ij)} = \partial Q^i/\partial P_t^j$ for example. With this result the monodromy matrixes need only be propagated in the reverse direction. We can thus finally weight each trajectory's contribution by the $C(\mathbf{P},\mathbf{Q},t)$ and preaveraging weight factors according to eq 15 to obtain our final results.

In strongly chaotic systems it may prove more fruitful to incorporate the positive definite, rapidly damping preaveraging weight factor $\exp[-\Delta\theta^2(\mathbf{P},\mathbf{Q})]$ into the importance sampling Monte Carlo procedure which we use to integrate over trajectory initial conditions. We are currently exploring such an approach for application to many body systems.

For studying our excited I_3 vibrational dynamics probed in I_3^- photodetachment experiments; however, the straightforward preaverage weighting procedure described above provides a reliable way to implement semiclassical expressions. In Figure 6, for example, we show that the spurious fragmentation of the wave function observed with the bare application of semiclassical propagation is completely remedied by use of the preaveraging procedures discussed above. The spurious effects of the high energy components of our ensemble which should be controlled by interference are effectively removed by the preaverage weighting procedure. We also see from Figure 5b a dramatic improvment in the time dependence of the energy components, and in energy conservation using this preaveraging approach.

We conclude this section with an observation on the relative amount of work involved in the semiclassical calculation of the thermal averaged time correlation given in eqs 5 and 12 as compared to its fully quantum mechanical calculation. As a result of our assumption that the initial states are prepared by exciting a thermal distribution of harmonic oscillator vibrational states in the ground electronic state well, each of these initial states has the form of a product of Gaussians times polynomials

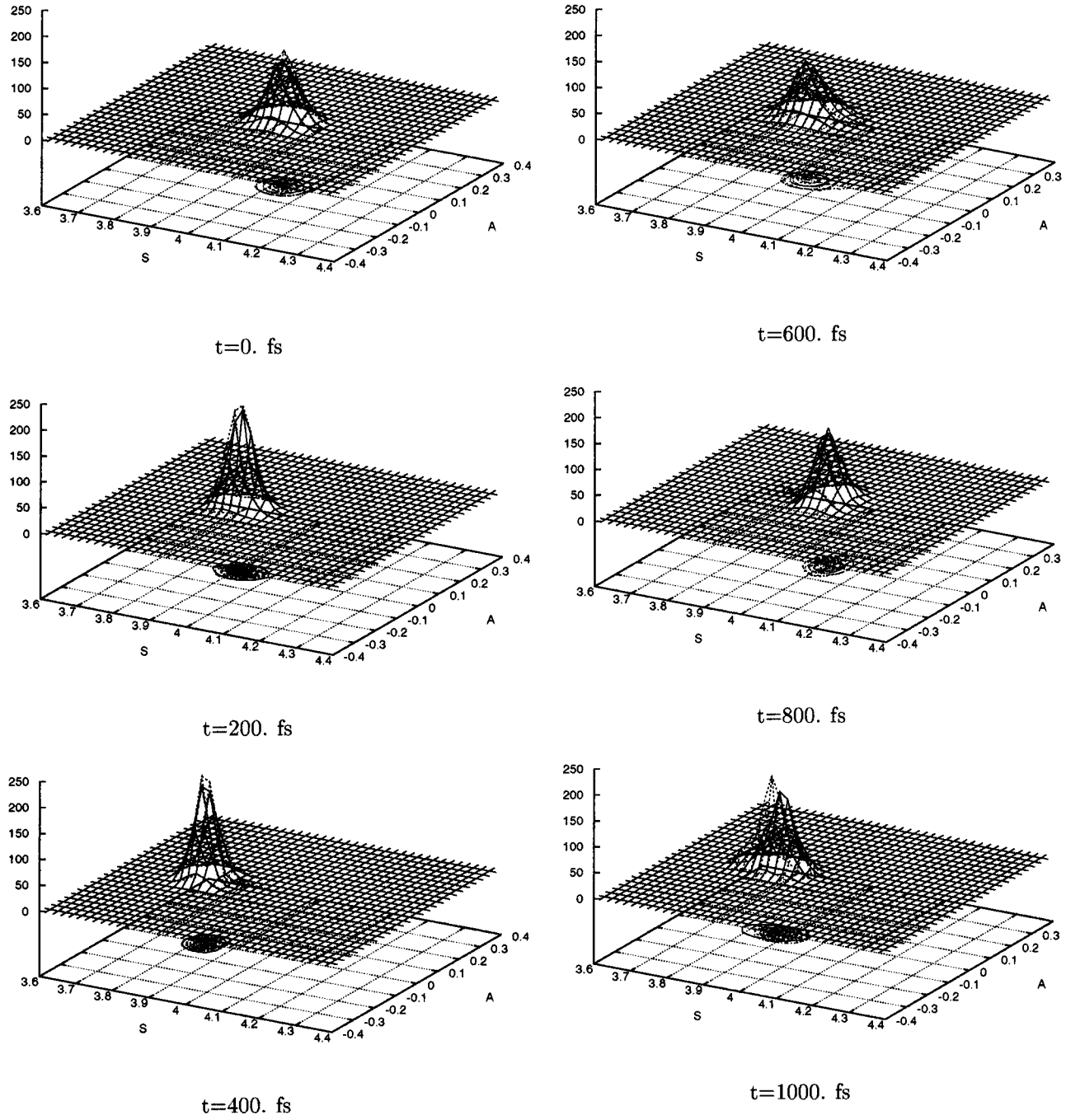

Figure 6. Propagation of initial harmonic I_3^- ground vibrational state on the photoexcited I_3 DIM potential surface. Surface of solid lines is propagated using the preaveraging approach for semiclassical algorithm. The dashed surface is the full quantum wavefunction propagated using split operator FFT methods. The wavefunctions are plotted as functions of symmetric and antisymmetric stretch normal modes in Ångstroms.

in the various normal modes of the ground state surface. For the full quantum calculation of the thermally weighted sum of correlation functions in eq 5 we must take each of the different thermally accessible initial states, evolve them subject to the nuclear Hamiltonian of the excited electronic state, and finally overlap the evolved function at time t with its initial state to obtain the component signal associated with this particular initial state. Correlation functions computed in this way must finally be weighted with the appropriate Boltzman factors and added to give the total correlation function as in eq 5. Thus if there are n thermally accessible states, we need to perform n propagations to construct our fully quantum thermal average.

For the semiclassical calculation described above, on the other hand, the propagation of all the different harmonic oscillator initial states can be accomplished by a SINGLE semiclassical propagation from the product Gaussian ground state initial distribution of position and momentum parameters (see the exponential factors in eq 13). Each of the different state contributions in this semiclassical representation of the dynamics is simply obtained by multiplying each trajectory's contribution by the appropriate product polynomials (see the polynomial factors in eq 13), and their complex conjugates, in the initial and final phase space points of the given trajectory and adding these trajectory contributions to the ensemble average. There is thus a qualitatively different amount of effort required for these quantal and semiclassical calculations due to fundamental differences in the nature of the quantal and semiclassical propagators and how they evolve wave functions. The same potential for savings

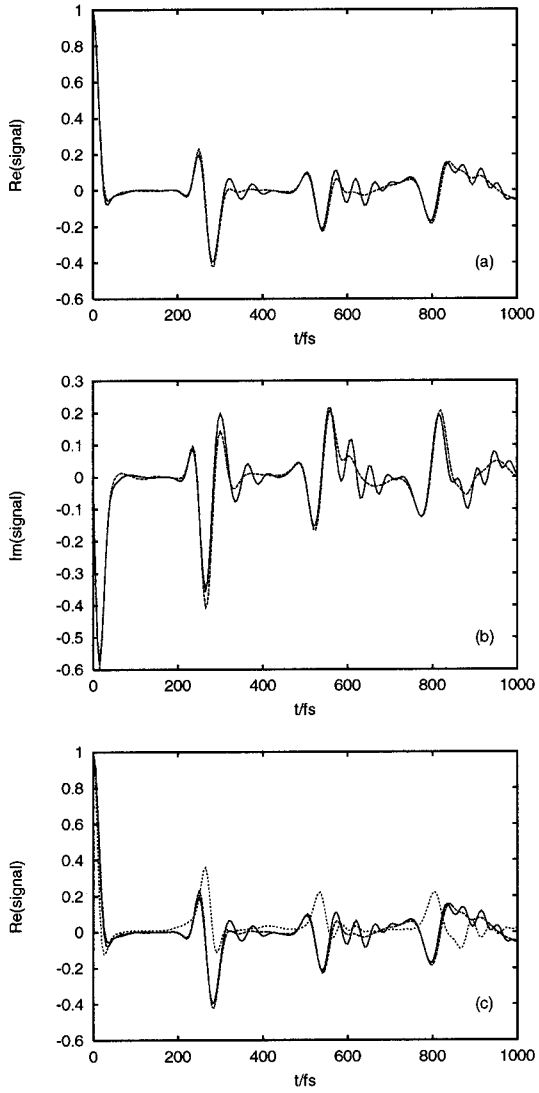

Figure 7. Parts a and b show real and imaginary parts of thermal averaged time correlation function $\phi_{IF}(t;\beta)$ defined in eq 5 for $T = 205$ *K*. Solid curves are full quantum calculations and dashed curves are preaveraged semiclassical calculations. Part c compares real part of correlation function computed with full quantum (solid curve), preaveraged semiclassical (dashed curve), and results obtained when the trajectory stability factors are ignored (dotted curve).

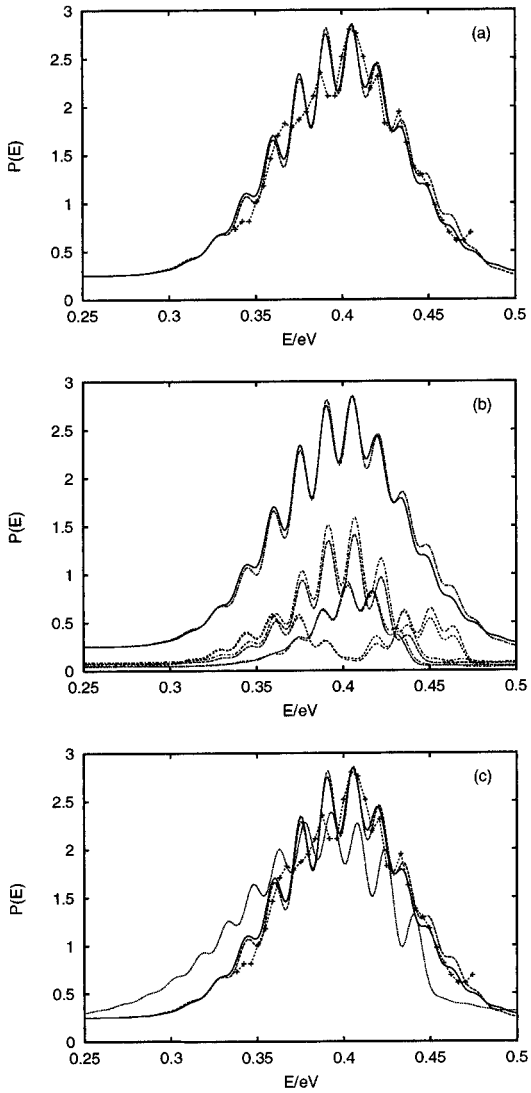

Figure 8. (a) Comparison of I_3^- photoelectron spectrum calculated with full quantum nuclear propagation (solid curve), preaveraged semiclassical nuclear propagation (dashed curve), and experimental curves (dotted curve with + symbols). (b) Comparison of full quantum and preaveraged semiclassical contributions to total signal. Upper curves are total signals, the three sets of component curves below these are contributions starting from the ground vibrational state $(S,A) = (0,0)$ (largest components), contributions from low initial symmetric stretch excitations, i.e., $\sum_{n=1}^{3}(n,0)$ (bimodal contributions), and contributions from low initial anti-symmetric stretch excitations, i.e., $\sum_{n=1}^{3}(0,n)$ (band with shifted peaks). (c) Same as that in part a only here we also include the result obtained when trajectory stability factors are ignored (shifted dotted curve).

in the semiclassical calculation of thermal averaged time correlation functions exists when ever the initial states can be written as a product of functions in the various coordinates and fast varying pieces of these functions can be pulled out as an initial phase space distribution for the parameters in a coherent state basis set representation and the remainder of the initial state functions are incorporated in multiplicative quantities to be averaged over initial and final points of classical trajectories as in eq 12. In future work we will explore the application of these ideas to study rotational dynamics.[35]

3. Results and Discussion

In Figure 7 we present our calculated thermal averaged time correlation functions as defined in eq 5 for the ground-state I_3 vibrational dynamics excited as a result of photoelectron detachment from ground-state I_3^-. For comparison we present the correlation function obtained from full quantum calculations as well as our preaverage weighted semiclassical results. Generally, the agreement between these calculated correlation functions is very good with the semiclassical results reproducing the general periodicity very accurately and smoothing out some of the finer details of the fully quantum signal. In the bottom part c of this figure we also compare the real part of the correlation function obtained by setting the *C* factor trajectory stability weights to unity. This is a commonly used approximation[36-38] which gives considerable numerical savings in semiclassical calculations. Unfortunately, as we see from this figure, the time correlation function obtained with this approximation for the vibrational dynamics of our I_3 system is really quite poor.

The time signals presented in Figure 7 can be transformed to energy space according to eq 4 giving the distributions of photoejected electron kinetic energies which we compare with the experimental results of Neumark and co-workers in Figure 8a. The calculated spectra presented in this figure were generated

assuming a Gaussian photoexcitation pulse width of $\tau = 100$ fs. The peak positions and band shape of the full quantum and semiclassical results agree with one another very closely and the overall shape of these calculated curves is in near quantitative agreement with the experimental results. The main deviations between the calculated and experimental results apparent in this figure are on the low energy side of the band where the calculated curves display a little too much structure and the peak positions may be shifted slightly. Generally, however, the close agreement with experiment is quite good.

In part b of Figure 8 we show a break down of our calculated signals into contributions from various initial states with in the thermal distribution. We see that the general shape of the final band results not only from contributions from the ($S = 0$, $A = 0$) or (0,0) ground vibrational state but there are also significant contributions from symmetric stretch excitations (n,0) which tend to broaden the band as they give contributions on either side of band center, and antisymmetric stretch excitations (0,n) which give slightly shifted contributions near the middle of the band. On the basis of these observations it is clear that several factors could be contributing to the small differences between the experimental and calculated spectra described above: First, with in the harmonic I_3^- initial surface approximation the hot bands line up, rather than being displaced due to anharmonicities. This will of course result in too much structure in the final spectrum. Next, uncertainty in the difference between the symmetric and antisymmetric stretch frequencies of the I_3^- initial surface can lead to an inaccurate representation of the interference between the peaks and troughs of the various contributions to the spectrum. Further, we have ignored the bending motions of the molecule and overlapping different bend vibration progressions could easily fill in the spaces between the bands we see in our restricted calculation results, thus smearing much of the detailed structure we observe. Our neglect of molecular rotations of course has a similar effect and including such motions would further smear out the features leading to closer agreement with experiment. Finally, if the shape of our DIM I_3 surface was inaccurate, our dynamics over this surface would fail give a good representation of the Franck−Condon factors responsible for controlling the amplitude of the various hot band contributions to the spectrum. Given all these potential problems, the fact that we get a spectrum which so closely resembles the experimental results is quite remarkable.

In the bottom part c of Figure 8 we compare the spectra from our quantum and semiclassical calculations with that obtained from ignoring the C trajectory stability factors. Not surprisingly, just as with the time correlation functions, leaving out these factors which account for the variation in semiclassical path space volume around each classical trajectory leads to significant errors.

4. Conclusions

In this paper we have presented a model potential describing the symmetric and antisymmetric stretch motions of a linear I_3 molecule obtained from a semiempirical diatomics-in-molecules approach. This model system has been employed as a test of various semiclassical methods for propagating nuclear vibrational wavefunctions over this highly anharmonic, weakly bound potential surface.

We have demonstrated the problems with implementing a bare semiclassical approach which involves a straightforward weighting of the contributions from various trajectories by a semiclassical approximation to the volume of path space around each classical trajectory. These approximate path space volumes are related to trajectory stability with respect to changes in initial conditions. In regions where the classical trajectories become chaotic this semiclassical approximation to the local path space volume thus diverges and we have demonstrated the disasterous effect of these chaotic trajectories at longer times in the application of the bare semiclassical approach with a finite ensemble of trajectories to this realistic two-dimensional model problem.

Contributions from these unstable trajectories should interfere destructively with other trajectories eminating from these chaotic regions as the integrand is highly nonstationary with respect to variations in trajectory initial conditions over which we integrate to obtain the semiclassical propagator. We have shown through comparison with exact full quantum calculations that the first order stationary phase filtering or preaveraging approach proposed by Herman[22,23] provides a simple to implement, potentially quite general, and extremely effective solution to this problem for our model system. We have further shown that the alternative approach to handling the contributions from chaotic trajectories in which we simply assume that the path space volume associated with all trajectories is a constant, independent of trajectory, yields poor dynamical results for this realistic problem.

Finally by comparing the ejected photoelectron kinetic energy distributions calculated from our semiclassical and quantum calculations with the experimental results of Neumark[1] we have demonstrated the remarkable accuracy of our semiempirical I_3 potential which gives reasonable estimates of the binding energies and stretch vibrational frequencies with no adjustable parameters.

5. Acknowledgment

We are grateful to Prof. Ruth Lynden-Bell for important discussions on limiting the DIM basis set size through symmetry requirements. We gratefully acknowledge financial support for this work from the National Science Foundation (Grant CHE9521793) and the Petroleum Research Fund of the American Chemical Society (Grant 34927-AC6). We also acknowledge a generous allocation of supercomputer time from the Boston University's center for Scientific Computing and Visualization.

6. Appendix

The time dependent perturbation theory approach we outline here to obtain the expression we use to calculate the photoelectron spectrum is very similar to that presented by Heller for the calculation of the Raman spectrum.[39] This approach is commonly used in many spectroscopic applications.[40]

The time dependent Hamiltonian describing the molecular ion in a classical radiation field is $\hat{H}(t) = \hat{H}_{\text{molec}} - \hat{\mu}\cdot\epsilon(t)$ where $\hat{\mu}$, for our molecular photoionization example, is the molecular ion dipole operator, $\epsilon(t)$ is the time dependent electric field, and $\hat{H}_{\text{molec}} = \hat{K}_N(\hat{\mathbf{P}}) + \hat{H}_{\text{el}}(\hat{\mathbf{p}},\hat{\mathbf{r}},\hat{\mathbf{R}})$ is the molecular ion Hamiltonian composed of the usual nuclear kinetic and electronic contributions. As usual we employ the Born−Oppenheimer adiabatic electronic eigenstates $\Phi_J(\mathbf{r},\mathbf{R})$ defined for a given nuclear configuration by $\hat{H}_{el}(\hat{\mathbf{p}},\hat{\mathbf{r}};\mathbf{R})\Phi_J(\mathbf{r},\mathbf{R}) = E_J(\mathbf{R})\Phi_J(\mathbf{r},\mathbf{R})$ as a basis set to represent the electronic distribution for nuclear configuration $\mathbf{R}$.

The time dependent wave function of the molecular ion coupled to the radiation field $\Psi(\mathbf{r},\mathbf{R},t)$ satisfies

$$i\hbar\frac{\partial}{\partial t}\Psi(\mathbf{r},\mathbf{R},t) = \hat{H}(t)\Psi(\mathbf{r},\mathbf{R},t) \tag{20}$$

Writing the solution of this equation in terms of the above adiabatic electronic basis set as

$$\Psi(\mathbf{r},\mathbf{R},t) = \sum_J \chi_J(\mathbf{R},t)\Phi_J(\mathbf{r},\mathbf{R}) \tag{21}$$

and making the Born−Oppenheimer approximation we find that if we arrange the nuclear coefficient functions $\chi_J(\mathbf{R},t)$ into a vector $\mathbf{X}(\mathbf{R},t)$ they satisfy the following matrix equation

$$i\hbar\frac{\partial}{\partial t}\mathbf{X}(\mathbf{R},t) = \hat{\mathbf{H}}(t)\mathbf{X}(\mathbf{R},t) \tag{22}$$

where $\hat{\mathbf{H}}(t) = \hat{\mathbf{H}}_0 + \mathbf{V}(t)$ is a matrix of nuclear Hamiltonians, the time independent part of which has elements $[\hat{\mathbf{H}}_0]_{IK} = \hat{H}_K\delta_{IK}$ where $\hat{H}_K = \hat{K}_N + E_K(\mathbf{R})$ is the Hamiltonian governing nuclear motion over the Born−Oppenheimer surface $E_K(\boldsymbol{R})$. The time dependent part of the matrix has elements$[\mathbf{V}(t)]_{IK} = -\epsilon(t)\cdot\mathbf{M}_{IK}(\mathbf{R})$ which describe how the radiation field couples the nuclear coefficient functions on different electronic surfaces. Here $\mathbf{M}_{IK}(\mathbf{R}) = \langle\Phi_I|\hat{\mu}|\Phi_K\rangle(\mathbf{R})$.

The first order time dependent perturbation theory solution of this system of equations is readily obtained as

$$\mathbf{X}(\mathbf{R},t) = \exp\left[-\frac{i}{\hbar}\hat{\mathbf{H}}_0(t-t_0)\right]\mathbf{X}(\mathbf{R},t_0) + \frac{1}{i\hbar}\int_{t_0}^{t}\mathrm{d}t' \times \exp\left[-\frac{i}{\hbar}\hat{\mathbf{H}}_0(t-t')\right]\mathbf{V}(t')\exp\left[-\frac{i}{\hbar}\hat{\mathbf{H}}_0(t'-t_0)\right]\mathbf{X}(\mathbf{R},t_0) \tag{23}$$

We assume that the system is prepared in some initial Born−Oppenheimer vibronic eigenstate $\chi_{I\mathbf{v}}(\mathbf{R})\Phi_I(\mathbf{r},\mathbf{R})$ where $\chi_{I\mathbf{v}}$ are the vibrational eigenstates of the nuclear Hamiltonian (specified by the vector $\mathbf{v}$ of vibrational quantum numbers) for electronic state I, i.e., $\hat{H}_I(\mathbf{R})\chi_{I\mathbf{v}}(\mathbf{R}) = E_{I\mathbf{v}}\chi_{I\mathbf{v}}(\mathbf{R})$ so the initial nuclear coefficient vector, $\mathbf{X}(\mathbf{R},0)$ has only a single nonzero entry, $\chi_{I\mathbf{v}}(\mathbf{R})$ as the Ith component function. Thus to first order in perturbation theory eq 23 gives that the nuclear coefficient function for the Jth electronic state at time t will be

$$\chi_J(\mathbf{R},t) = \exp\left[-\frac{i}{\hbar}\hat{H}_I(t-t_0)\right]\chi_{IJ}(\mathbf{R})\delta_{IJ} + \frac{1}{i\hbar}\int_{t_0}^{t}\mathrm{d}t' \times \exp\left[-\frac{i}{\hbar}\hat{H}_J(t-t')\right]V_{JI}(t')\exp\left[-\frac{i}{\hbar}\hat{H}_I(t'-t_0)\right]\chi_{I\mathbf{v}}(\mathbf{R}) \tag{24}$$

For our photoelectron experiment described in subsection 2.2 $\Phi_J = \Phi_{F\epsilon}$ so $\hat{H}_J(\mathbf{R}) = \hat{H}_F(\mathbf{R}) + \epsilon$. Thus the probability of observing a photoelectron with kinetic energy ϵ and depositing the system in neutral state F at time t from a molecular ion prepared in state $I\mathbf{v}$ before time t_0 when a radiation field was applied is obtained from the square of the above amplitude as

$$P(F\epsilon,I\mathbf{v},t) = \frac{1}{\hbar^2}\int_{t_0}^{t}\mathrm{d}t'\int_{t_0}^{t}\mathrm{d}t''\exp\left[-\frac{i}{\hbar}(\epsilon - E_{I\mathbf{v}})(t''-t')\right]V_{IF\epsilon}(t'')V_{F\epsilon I}(t') \times \left\langle\chi_{I\mathbf{v}}\right|\exp\left[-\frac{i}{\hbar}\hat{H}_F(t''-t')\right]\left|\chi_{I\mathbf{v}}\right\rangle \tag{25}$$

In writing this result we have made the Condon approximation and assumed that the dipole matrix elements vary weakly with nuclear configuration so $V_{IF\epsilon}$, etc., is approximately independent of $\mathbf{R}$.

We further suppose that the excitation pulse at frequency ω has a Gaussian time profile with experimental width parameter τ, so that $V_{IF\epsilon}(t) = A_{IF\epsilon}\exp[-t^2/2\tau^2]\cos\omega t$. Transforming the double time integral to sum and difference times, and extending t_0 to $-t$, we can perform the integration over the sum variable analytically and keeping only the resonant term we find the infinite time probability of observing a photoelectron with energy ϵ resulting from the transition $F \leftarrow I\mathbf{v}$ is obtained as

$$P(F\epsilon,I\mathbf{v},\infty) \sim \frac{|A_{IF\epsilon}|^2}{\hbar^2}\mathrm{Re}\left\{\int_0^\infty \mathrm{d}s\exp\left[-\frac{i}{\hbar}(\epsilon - E_{I\mathbf{v}} - \hbar\omega)s\right] \times \exp\left[-\frac{s^2}{4\tau^2}\right]\left\langle\chi_{I\mathbf{v}}\right|\exp\left[-\frac{i}{\hbar}\hat{H}_F s\right]\left|\chi_{I\mathbf{v}}\right\rangle\right\} \tag{26}$$

Finally the total probability, $P_\beta(\epsilon)$ of observing ejected photoelectrons with kinetic energy ϵ at long time if the molecules are initially in thermal equilibrium at a temperature T, which is proportional to the signal in these experiments, is obtained by summing over a Boltzman distribution of initial states and adding the signal contributions from all possible final states, thus

$$P_\beta(\epsilon) = \sum_{I\mathbf{v}}\exp[-\beta E_{I\mathbf{v}}]\sum_F P(F\epsilon,I\mathbf{v},\infty) \tag{27}$$

where $\beta = 1/k_\mathrm{B}T$.

In our calculations we assume that the ground electronic state of our molecular anion system is well separated from any excited electronic states so the Boltzman contributions from these higher energy electronic states can be ignored and we need only sum over initial excited vibrational states on the ground electronic state surface. Further, we will suppose that the final excited electronic states of interest, which involve only the ground state of the neutral molecule and the ejected electron with various amounts of kinetic energy, are sufficiently well separated from other excited neutral states so these higher excited final states can be neglected for the ground-state to ground-state band we wish to study.

Note in this work we assume that the quantities $|A_{IF\epsilon}|^2$ are weakly varying functions of electronic kinetic energy ϵ, compared to the time integral in eq 26. Finally, we have adjusted our calculated spectrum so that its peak amplitude matches experiment for purpose of comparison.

References and Notes

(1) Taylor, T. R.; Asmis, K. R.; Zanni, M. T.; Neumark, D. M. *J. Chem. Phys.* **1999**, *110*, 7607.

(2) Batista, V. S.; Coker, D. F. *J. Chem. Phys.* **1996**, *105* 4033.

(3) It is possible that the ground state of I_3 has $M_J = \pm^3/_2$. Some of the states with this angular momentum projection will have the same dissociation limit as the $M_J = \pm^1/_2$ which we assume to be the ground state in this analysis. These states are currently under investigation and may lie close in energy to our assumed ground state. The experiments may probe a statistical distribution of the various states.

(4) Ellison, F. O. *J. Am. Chem. Soc.* **1963**, *85*, 3540.

(5) Tully, J. C. In *Semiempirical Methods of Electronic Structure Calculation, Part A: Techniques*; Segal, L. A., Ed.; Plenum: New York, 1977.

(6) Ruhman, S.; Lynden-Bell, R.; Kosloff, R.; Vala, J. *J. Chem. Phys.* **1998**, *109*, 9928.

(7) Sato, H.; Hirata, F.; Myers, A. B. *J. Phys. Chem. A* **1998**, *102*, 2065.

(8) Feit, M. D., Jr.; Fleck, J. A.; Steiger, A. *J. Comput. Phys.* **1982**, *47*, 412.

(9) Kosloff, R. *J. Phys. Chem.* **1988**, *92*, 2087.

(10) Herman, M. F.; Kluk, E. *Chem. Phys.* **1984**, *91*, 27.

(11) Kluk, E.; Herman, M. F.; Davis, H. L. *J. Chem. Phys.* **1986**, *84*, 326.

(12) Kay, K. G. *J. Chem. Phys.* **1994**, *100*, 4377.

(13) Kay, K. G. *J. Chem. Phys.* **1994**, *100*, 4432.

(14) Kay, K. G. *J. Chem. Phys.* **1994**, *101*, 2250.

(15) Kay, K. G. *J. Chem. Phys.* **1997**, *107*, 2313.

(16) Madhusoodanan, M.; Kay, K. G. *J. Chem. Phys.* **1998**, *109*, 2644.

(17) Lichtenberg, L.; Lieberman, M. In *Computer Simulation in Chemical Physics*; Springer-Verlag: New York, 1983.
(18) Heller, E. J. *J. Chem. Phys.* **1991**, *94*, 2723.
(19) Walton, A. R.; Manolopoulos, D. E. *Chem. Phys. Lett.* **1995**, *244* 448.
(20) Walton, A. R.; Manolopoulos, D. E. *Mol. Phys.* **1996**, *87*, 961.
(21) Hulme, J.; Brewer, M.; Manolopoulos, D. E. *J. Chem. Phys.* **1997**, *106*, 4832.
(22) Herman, M. F.; Guerin, B. *Chem. Phys. Lett.* **1998**, *286*, 361.
(23) Herman, M. F. *Chem. Phys. Lett.* **1997**, *275*, 445.
(24) Campolieti, G.; Brumer, P. *J. Chem. Phys.* **1998**, *109*, 2999.
(25) Elran, Y.; Kay, K. G. *J. Chem. Phys.* **1990**, *110*, 3653.
(26) Herman, M. F.; Coker, D. F. *J. Chem. Phys.* **1999**, *111*, 1801.
(27) Filinov, V. S. *Nucl. Phys. B* **1986**, *271*, 717.
(28) Makri, N.; Miller, W. H. *Chem. Phys. Lett.* **1987**, *139*, 10.
(29) Makri, N.; Miller, W. H. *J. Chem. Phys.* **1988**, *89*, 2170.
(30) Coalson, R. D.; Freeman, D. L.; Doll, J. D. *J. Chem. Phys.* **1986**, *85*, 4567.
(31) Doll, J. D.; Freeman, D. L.; Gillan. M. J. *Chem. Phys. Lett.* **1988**, *143*, 277.
(32) Spath,B. W.; Miller, W. H. *J. Chem. Phys.* **1996**, *104*, 95.
(33) Garashchuk, S.; Tannor, D. J. *Chem. Phys. Lett.* **1996**, *262*, 477.
(34) Herman, M. F. *J. Chem. Phys.* **1986**, *85*, 2069.
(35) Xiong Sun; Miller, W. H. *J. Chem. Phys.* **1998**, *108*, 8870.
(36) Ovchinnikov, M.; Apkarian, V. A. *J. Chem. Phys.* **1997**, *106*, 5775.
(37) Ovchinnikov, M.; Apkarian, V. A. *J. Chem. Phys.* **1998**, *108*: 2277.
(38) Ovchinnikov, M.; Apkarian, V. A. *J. Chem. Phys.* **1996**, *105*: 10312.
(39) Lee, S. Y.; Heller, E. J. *J. Chem. Phys.* **1979**, *71*, 4777.
(40) Batista, V. S.; Zanni, M. T.; Greenblatt, B. J.; Neumark, D. M.; Miller, W. H. *J. Chem. Phys.* **1999**, *110*, 3736.